Journal of
Mechanics of
Materials and Structures

DYNAMIC COMPRESSION OF SQUARE HONEYCOMB STRUCTURES DURING UNDERWATER IMPULSIVE LOADING

Haydn N. G. Wadley, Kumar P. Dharmasena, Doug T. Queheillalt, YungChia Chen, Philip Dudt, David Knight, Ken Kiddy, Zhenyu Xue and Ashkan Vaziri

Volume 2, Nº 10 December 2007

mathematical sciences publishers

JOURNAL OF MECHANICS OF MATERIALS AND STRUCTURES
Vol. 2, No. 10, 2007

DYNAMIC COMPRESSION OF SQUARE HONEYCOMB STRUCTURES DURING UNDERWATER IMPULSIVE LOADING

HAYDN N. G. WADLEY, KUMAR P. DHARMASENA, DOUG T. QUEHEILLALT, YUNGCHIA CHEN, PHILIP DUDT, DAVID KNIGHT, KEN KIDDY, ZHENYU XUE AND ASHKAN VAZIRI

Significant reductions in the fluid structure interaction regulated transfer of impulse occur when sandwich panels with thin (light) front faces are impulsively loaded in water. A combined experimental and computational simulation approach has been used to investigate this phenomenon during the compression of honeycomb core sandwich panels. Square cell honeycomb panels with a core relative density of 5% have been fabricated from 304 stainless steel. Back supported panels have been dynamically loaded in through thickness compression using an explosive sheet to create a plane wave impulse in water. As the impulse was increased, the ratio of transmitted to incident momentum decreased from the Taylor limit of 2, for impulses that only elastically deformed the core, to a value of 1.5, when the peak incident pressure caused inelastic core crushing. This reduction in transmitted impulse was slightly less than that previously observed in similar experiments with a lower strength pyramidal lattice core and, in both cases, was well above the ratio of 0.35 predicted for an unsupported front face. Core collapse was found to occur by plastic buckling under both quasistatic and dynamic conditions. The buckling occurred first at the stationary side of the core, and, in the dynamic case, was initiated by reflection of a plastic wave at the (rigid) back face sheet-web interface. The transmitted stress through the back face sheet during impulse loading depended upon the velocity of the front face, which was determined by the face sheet thickness, the magnitude of the impulse, and the core strength. When the impulse was sufficient to cause web buckling, the dynamic core strength increased with front face velocity. It rose from about 2 times the quasistatic value at a front face initial velocity of 35 m/s to almost 3 times the quasistatic value for an initial front face velocity of 104 m/s. The simulations indicate that this core hardening arises from inertial stabilization of the webs, which delays the onset of their buckling. The simulations also indicate that the peak pressure transmitted to a support structure from the water can be controlled by varying the core relative density. Pressure mitigation factors of more than an order of magnitude appear feasible using low relative density cores. The study reveals that for light front face sandwich panels the core strength has a large effect upon impulse transfer and the loading history applied to support structures.

1. Introduction

Metallic sandwich panels with cellular cores have attracted significant attention for dynamic energy absorption and impact mitigation [Baker et al. 1998; Fleck and Deshpande 2004; 2005; Hutchinson and Xue 2005; Deshpande et al. 2006; Rathbun et al. 2006; Dharmasena et al. 2007b; Liang et al. 2007]. During impact with rigid objects, they reduce damage to the structures they protect by core crushing and face sheet stretching at pressures significantly less than those created when an equivalent solid is

Keywords: sandwich panels, honeycomb cores, impulse loading, cellular structures.

impacted. When sandwich panel structures are impulsively loaded in water, additional mitigation is possible because of beneficial fluid structure interactions (FSI) with thin face sheets [Fleck and Deshpande 2004; Hutchinson and Xue 2005].

The origin of the FSI enhancement arises from a reduction in the reflection coefficient of a normally incident shock front with a solid structure. The pressure pulse from a detonation in water exhibits a sharp rise to a peak pressure and is followed by a slower decay [Cole 1948]. The pressure, $p(t)$, can be written

$$p(t) = p_0 e^{-t/t_0},$$

where p_0 is the peak pressure, t is time measured from the peak in pressure and t_0 is a characteristic time constant. The impulse per unit area, I_0, transported by the pressure pulse through the fluid is given by

$$I_0 = \int_0^\infty p(t)dt = p_0 t_0.$$

Taylor [1963] showed that in the linear (acoustic) fluid propagation limit, the pressure pulse is totally reflected at the surface of a rigid structure, or one with very heavy face sheets. The impulse I transmitted to the structure is then twice that of the incident pulse. An extension of Taylor's theory for FSI in air blasts, which accounts for nonlinear compressibility and finite shock behavior, was recently proposed [Kambouchev et al. 2006] and employed to assess the performance of all-metal sandwich plates under high intensity air shocks [Vaziri and Hutchinson 2007]. In this the reflection coefficient depends upon the peak pressure, and can reach a value of 8 for ideal gases, and higher values when dissociation occurs.

When an unsupported thin (light) panel or a sandwich panel with thin faces and a very weak core is impulsively loaded in water, the front face sheet can move away from the impulse, and the transmitted pressure and impulse are then less than the Taylor prediction [Taylor 1963; Fleck and Deshpande 2004; Hutchinson and Xue 2005]. The effect is strongest for water borne impulses. In the acoustic limit, the transmitted impulse I when a core has no strength depends only upon the thickness of the front face sheet, the density of the material it is made of, and the decay time (t_0) of the pulse, as

$$I = 2I_0 q^{q/(1-q)}, \tag{1}$$

where

$$q = \frac{\rho_w c_w}{\rho h_f} t_0,$$

in which ρ_w is the density of and c_w the speed of sound in the acoustic medium, and ρ is the density and h_f the thickness of the face sheet. The mass per unit area of the face sheet, m_f, is the ρh_f product. The ratio $\rho_w c_w / m_f$ is an important dimensionless quantity which controls the impulse transferred to a plate structure. For very heavy plates, Equation (1) gives Taylor's result, but for thinner plates, large reductions in impulse can occur. For example, a 5 mm thick, 304 stainless steel plate loaded in water has $m_f = 40\,\mathrm{kg/m^2}$, $\rho_w = 1000\,\mathrm{kg/m^3}$, and $c_w = 1400\,\mathrm{m/s}$. If $t_0 = 0.1\,\mathrm{ms}$, $q = 3.5$, and the impulse transmitted from water to such a face sheet is only 0.35 times that of the incident pulse.

In sandwich panels with strong cores, front face sheet motion is resisted by the core [Xue and Hutchinson 2006; Liang et al. 2007]. Recent measurements of the impulse transmitted into fully back supported sandwich panels with pyramidal lattice cores and 4.8 mm thick stainless steel face sheets indicate the

transmitted to incident impulse ratio is increased (from 0.35 for a free 5 mm thick plate) to ~ 1.4 during underwater impulsive loading [Wadley et al. 2007a]. This is significantly less than the Taylor result for the rigid plate of the same mass per unit area as the sandwich panel. This result indicates that even when the face sheet thickness is held constant, considerable changes in the impulse transferred to a back supported structure can result from variations to the core crush resistance.

Recent analytical and numerical studies of edge supported panels subjected to dynamic loading have confirmed that core crushing during distributed impulsive loading does affect impulse transfer [Baker et al. 1998; Fleck and Deshpande 2004; 2005; Hutchinson and Xue 2005; 2006; Rathbun et al. 2006; Tilbrook et al. 2006; Dharmasena et al. 2007b; Liang et al. 2007; McShane et al. 2007]. This crushing behavior depends upon the cell topology, the material used to construct the cells, and the volume fraction of cell material (the core relative density, $\bar{\rho}$) [Tilbrook et al. 2006; McShane et al. 2007]. Numerous sandwich panel core topologies have been investigated, including simple I cores [Liang et al. 2007], various honeycombs [Xue and Hutchinson 2004; 2006; Dharmasena et al. 2007b], (prismatic) corrugations [Xue and Hutchinson 2004; Dharmasena et al. 2007a; McShane et al. 2007], and lattice truss structures [Wadley et al. 2007a; Wei et al. 2007a]. Examples of these are schematically illustrated in Figure 1. These theoretical assessments are being complimented with a variety of experiments designed to probe the dynamic crush response of cellular structures. This required development of experimental methods for the fabrication of sandwich panels from high ductility alloys [Tilbrook et al. 2006; McShane et al. 2007]. Honeycombs with cell dimensions in the 10 mm range can be made using a slotted sheet method followed by transient liquid phase bonding [Wadley et al. 2003; Wadley 2006]. The corrugations and lattices shown in Figure 1 can be made using sheet folding methods (in the latter case using a perforated metal sheet) [Wadley et al. 2003; Wadley 2006].

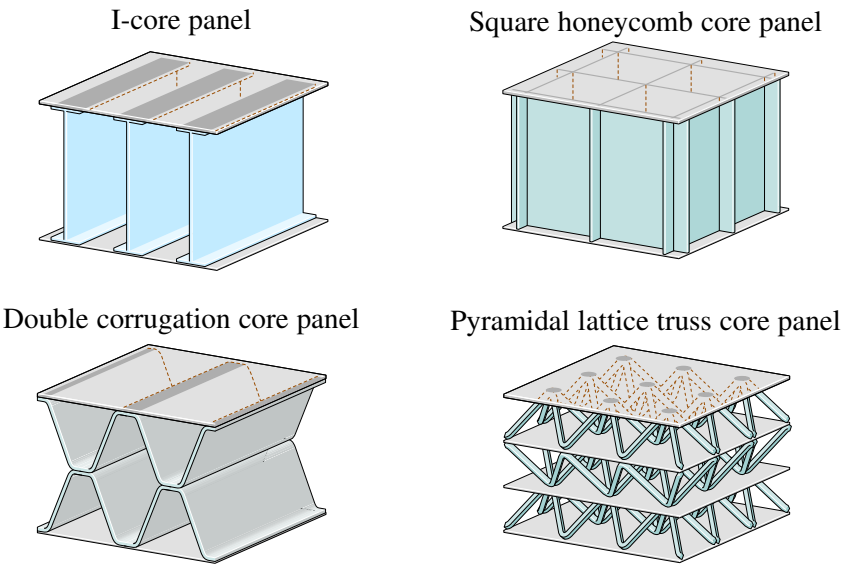

Figure 1. Cellular core topologies.

Several experimental techniques can be utilized to investigate the dynamic mechanical response of sandwich panel structures [Radford et al. 2005; Lee et al. 2006a; 2006b; Rathbun et al. 2006; Dharmasena et al. 2007b; Mori et al. 2007; Wadley et al. 2007a]. These include Kolsky bar methods [Lee et al. 2006a; 2006b] and gas gun experiments using metal foam projectiles [Radford et al. 2005; Rathbun et al. 2006] and other impactors [Lee et al. 2006a; 2006b; Mori et al. 2007]. These have been coupled with high speed photography to observe core crush mechanisms over a wide range of strain rates and incident pressures [Radford et al. 2005; Lee et al. 2006a; 2006b; Rathbun et al. 2006; Mori et al. 2007]. Recent water shock tube experiments have also been conducted on small scale metallic test structures with either stochastic foam [Radford et al. 2005; Deshpande et al. 2006], pyramidal lattice [Lee et al. 2006a; Mori et al. 2007], or square honeycomb [Rathbun et al. 2006; Mori et al. 2007] core topologies. These have enabled the dynamic response of sandwich panel structures to be examined as a function of the front face velocity (core crushing rate). All of these experiments indicate significant elevations of the quasistatic core strength once the front face velocity is increased above about 20 m/s [Deshpande et al. 2006].

Experimental assessments of the core dynamic compressive strength of sandwich panels can also be made using a novel explosive test technique, in which an explosive sheet is detonated inside a water column positioned on top of a well supported sandwich panel [Wadley et al. 2007a]. The response of the sandwich panel to the water borne impulse is then controlled by the charge mass, the charge to sample (standoff) distance, and the FSI which defines the momentum transferred to the structure [Fleck and Deshpande 2004; Hutchinson and Xue 2005; Liang et al. 2007]. The momentum transferred to the front face of the sandwich panels in these tests depends in part upon the face sheet mass per unit area [Hutchinson and Xue 2005; Liang et al. 2007]. As the momentum is acquired, the face sheet is quickly accelerated to a peak velocity. The characteristic time for this is governed by the decay constant of the exponentially decreasing pressure pulse [Cole 1948]. Movement of the front face compresses the core; the front face is decelerated by the dynamic resistance force of the core and eventually brought to rest. This resisting pressure can be measured at the back face, providing a good estimate of the core's dynamic compressive strength.

Finite element models (FEM) have been used to investigate the mechanisms of core crushing during dynamic loading [Qiu et al. 2003; Rabczuk et al. 2004; Xue and Hutchinson 2004; Xue et al. 2005; Tilbrook et al. 2006; Liang et al. 2007; McShane et al. 2007; Vaziri and Xue 2007]. The inelastic deformation of the axially loaded webs in a honeycomb panel begins by propagation of a plastic wave down the plate. If the back of the structure can support stress, reflection of the wave at the bottom face sheet can cause a buckle to form near the bottom face sheet [Vaughn and Hutchinson 2006]. Dynamic core hardening then results from three mechanisms: inertial resistance (to acceleration) of the core mass, inertial stabilization against web buckling, and material strain rate hardening of the webs [Xue and Hutchinson 2006]. The FEM analyses indicate that the three effects combine to dissipate the kinetic energy acquired by an impulsively loaded sandwich panel structure.

The energy absorbed during the crushing of a square honeycomb lattice increases with the critical buckling strain and is therefore sensitive to the mode of web collapse [Xue and Hutchinson 2006]. This depends upon the web thickness, width and height (which also establish the cell size and relative density), and the tangent modulus of the web material. Moreover, combining with an eigenvalue analysis, Xue and Hutchinson [2006] have also conducted a set of computations to systematically explore the effects of initial imperfection on the dynamic response of square honeycomb cores. They concluded that the

velocity imparted to the front face also plays a significant role in governing the buckling mode of web collapse such that the higher the velocity the shorter the buckling wavelength.

These studies reveal that the effective crush strength of a honeycomb core structure is a strong function of the velocity of the front face during dynamic loading. For small crush strains, motion of the front face is resisted by the reaction forces created when a plastic wave is propagated along the straight webs. If strain hardening effects are weak, and therefore ignored, the dynamic strength of the core in the nonbuckling regime is governed by the core's dynamic yield stress, σ^c_{YD}. In the plastic yield region of core crushing, this can be estimated by

$$\sigma^c_{YD} \cong \sigma_{YD}\bar{\rho},$$

where σ_{YD} is the dynamic yield strength of the alloy and $\bar{\rho}$ is the relative density of the core defined as the volume fraction of the core occupied by the material. The dynamic strength of 304 stainless steel at the loading rates of interest is not more than 20% higher than that measured quasistatically [Stout and Follansbee 1986].

At higher impulses, web buckling is the dominant deformation mode. The analysis of honeycomb web buckling from [Xue and Hutchinson 2006] led to the approximate relation between the dynamic yield strength and core density

$$\sigma^c_{YD} \cong \left[1 + \left(\frac{E_t}{E}\right)^{1/2}\left(\frac{v_f}{c_{el}\varepsilon_Y} - 1\right)\right]\sigma_Y\bar{\rho}, \tag{2}$$

where E_t is the linear hardening tangent modulus (measured quasistatically), E is the Young's modulus, c_{el} is the elastic wave speed, v_f is the front face (crush) velocity, and σ_Y and ε_Y are the yield strength and strain of the alloy, respectively. Equation (2) indicates that for fixed E and $\bar{\rho}$, it is beneficial to use alloys with high E_t. Austenitic stainless steels exhibit this characteristic.

Here we use a simple corrugation method to fabricate square honeycomb sandwich panel structures from a high ductility, high tangent modulus 304 stainless steel [Stout and Follansbee 1986], explained in Section 2. In Section 3, the quasistatic compression response of the core has been measured and found to be approximately three times stronger than the recently tested pyramidal lattice structures made from the same alloy [Wadley et al. 2007a]. It therefore provides an opportunity to experimentally assess the role of core strength (via a change in topology) upon impulse transmission during explosive loading. Test panels with identical thickness face sheets to those of the pyramidal lattice were subjected to a range of impulsive loads by varying the stand off distance between the test structure and a planar explosive source (see Section 3). The backside pressure-time waveforms of the fully back supported test structures were then monitored as they dynamically collapsed. Similar experiments were conducted with solid cylinders to determine the incident impulse. A complementary numerical modeling study investigated various aspects of the mechanical response of square honeycomb cores under this high intensity loading. A 3-dimensional finite element model of the experimental setup was constructed, and is described in detail in Section 4.1. The material models used in the computational schemes to represent the behavior of the water column and sandwich panel material are discussed in Section 4.2. In Section 4.3, a finite element hydrocode analysis was carried out to predict the pressure applied to the panel due to the underwater explosion. Finally, in Section 4.4, a simplified finite element unit cell model was used to investigate the effect of core relative density upon the dynamics of the square honeycomb core. These

finite element calculations were carried out using the commercially available software ABAQUS/Explicit. Experimental and numerical results are presented in Section 5 followed by a discussion of the results. The study confirms significant, front face velocity dependent core strengthening in square honeycomb structures. However, even though the dynamic honeycomb core strength is more than three times that of pyramidal lattices, the impulse transferred to heavily loaded panels is only increased slightly. The transmitted pressure appears controllable over wide ranges by varying the core density.

2. Sandwich panel fabrication

A sheet bending and brazing method was used to fabricate square honeycomb core sandwich panels from 304 stainless steel (see Figure 2). The core was fabricated by periodically bending 0.76 mm thick, 99 mm wide steel sheet to create a corrugated structure with a 90° bend angle. The peak to peak corrugation height was approximately 22 mm. Twelve of these corrugated panels were spot welded to create a square honeycomb block. A brazing paste (Wall Colmonoy, Nicrobraz 51 alloy) was applied along the contact edges. This assembly was placed between a pair of 4.8 mm thick, 304 stainless steel face plates which had been spray coated with the same brazing alloy powder carried in a polymer binder. Four structures were placed in a vacuum furnace and subjected to a high-temperature brazing treatment. The thermal cycle consisted of heating at 10° C/min to 550° C, holding for 20 minutes (to volatilize and remove the polymer binder), then further heating to 1050° C for 60 minutes at a base pressure of $\sim 10^{-4}$ torr before furnace cooling to ambient temperature at $\sim$ 25° C/min. After brazing, 203 mm diameter cylindrical samples were cut using a wire electro discharge machine to obtain the circular test samples for quasistatic and dynamic testing. A photograph of one of the test structures is shown in Figure 3.

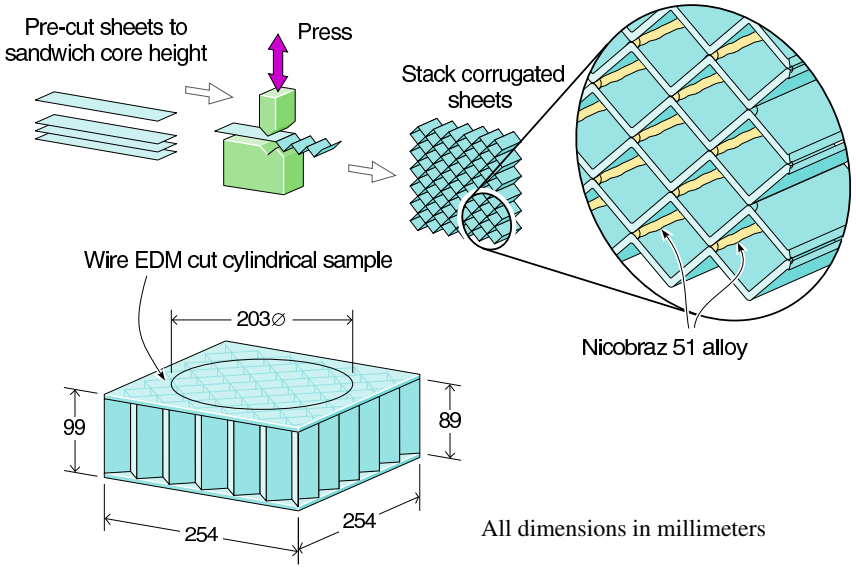

Figure 2. Square honeycomb core and sandwich panel fabrication process.

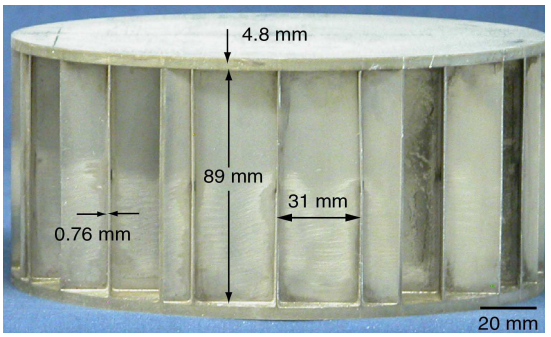

Figure 3. 304SS square honeycomb "dynocrusher" test sample.

The relative density, $\bar{\rho}$, of a square honeycomb structure can be calculated from the ratio of the metal to unit cell volumes (see Figure 4),

$$\bar{\rho} = \frac{t(2l - t)}{l^2} \cong 2\frac{t}{l}.$$

For the samples fabricated here, $h = 89$ mm, $l = 31$ mm, and $t = 0.76$ mm. This gives a core relative density of $\sim 5\%$.

3. Quasistatic compression and impulse loading tests

3.1. ***Alloy mechanical properties.*** The fabrication process resulted in a core made of annealed 304 stainless steel. The yield strength and strain hardening characteristics of this alloy are sensitive to its thermal history so the uniaxial stress strain response of similarly heat treated alloy specimens was measured according to ASTM E8-01 specifications at a strain rate of $10^{-4}\,\mathrm{s}^{-1}$. The elastic modulus and 0.2% offset yield strength were 203 GPa and 176 MPa, respectively. The strain hardening was well approximated by a bilinear fit to the true stress strain data up to a strain of 20%. The tangent modulus in this strain region was ~ 2.1 GPa.

3.2. ***Quasistatic compression.*** One sandwich panel sample was loaded in uniaxial compression at a strain rate of $5 \times 10^{-4}\,\mathrm{s}^{-1}$; its normalized stress strain response is shown in Figure 5a. The specimen

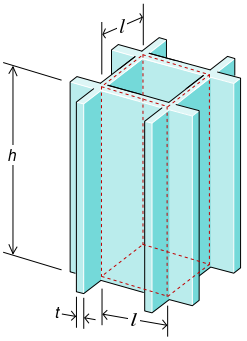

Figure 4. Square honeycomb core unit cell.

exhibited a peak strength of 12 MPa coincident with the onset of web buckling (marked by the first arrow). Two additional buckles were formed at strains of $\sim 25\%$ and $\sim 50\%$ before the core began to harden rapidly at a strain of $\sim 70\%$. The first buckling event occurred near the bottom (stationary) end of the sample. Figure 5b shows a cross section of the fully compressed sample. The onset of hardening at a strain of 70% resulted from the impingement of the three buckles in each honeycomb web.

3.3. ***Dynamic loading tests.*** The dynamic response of the square honeycomb structures was determined using the explosive test technique schematically illustrated in Figure 6. The test procedures were identical to those previously reported [Wadley et al. 2007a]. Each test sample was placed on a specimen tray resting on four high strength steel columns to which strain gauges were attached as shown. Prior calibrations in a mechanical testing frame were used to convert the strain gauge signals to average pressure measured at the back face of the specimen. Suitable band pass filtering techniques were used to increase the signal to noise ratio. A steel cover plate was positioned over the specimen such that the top sample face was flush with the top surface of the cover plate. A 0.9 m diameter cardboard cylinder (and plastic liner) was then placed over the cover plate and filled with water. A 20.3 cm $\times$ 20.3 cm $\times$ 0.1 cm explosive sheet was then positioned in the water at standoff distances $H = 25.4$ cm, 15.2 cm, or 10.2 cm above the top sample surface. An analysis of the test and effects of the reverberations in the support columns upon the results is presented elsewhere [Dharmasena et al. 2007a; Wei et al. 2007a].

3.4. ***Dynamic test calibration.*** The dynamic pulse loading system was calibrated using a solid 6061-T6 aluminum alloy cylinder whose outer dimensions were identical to the sandwich panel specimens. The

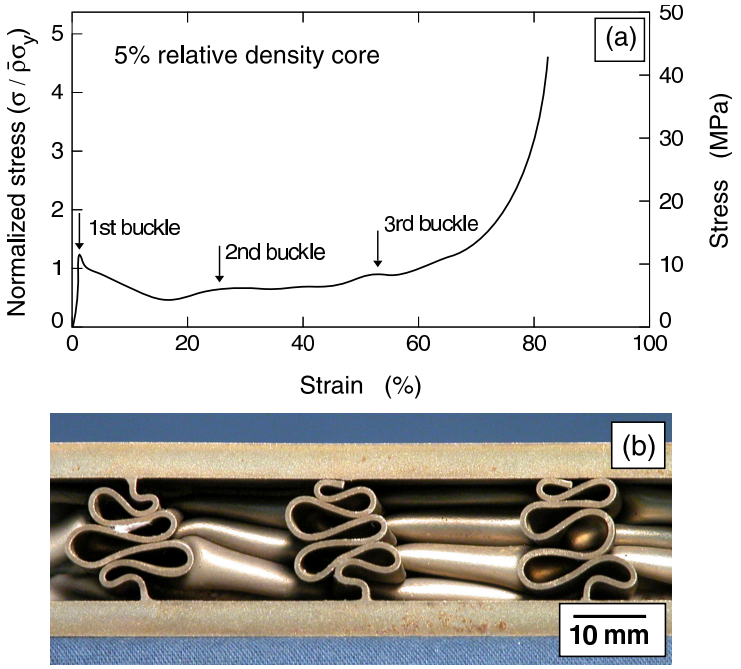

Figure 5. (a) Quasistatic response of 5% relative (core) density square honeycomb sample. (b) Compressed sample after quasistatic test.

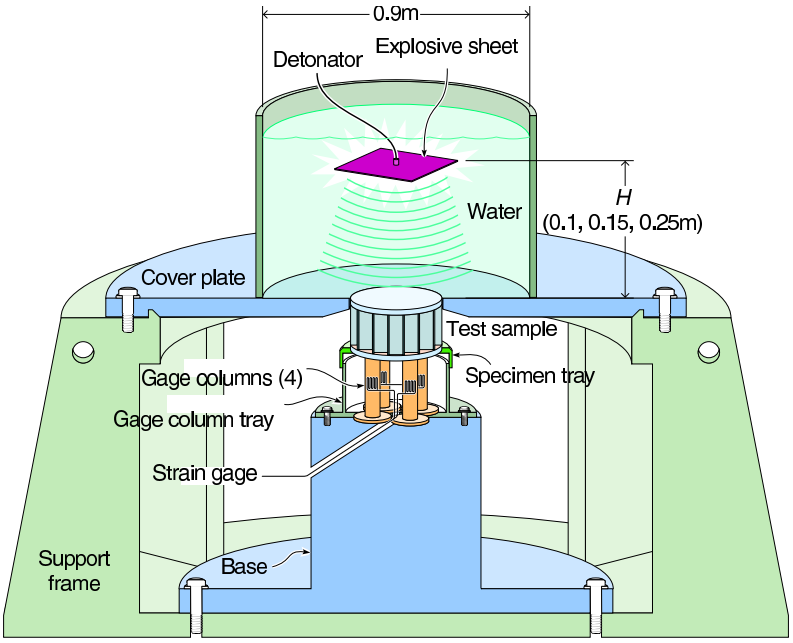

Figure 6. "Dynocrusher" test configuration.

"dry" side pressure for each test was obtained from the average of the four pressures converted from the strain gage signals. Each of the pressure-time traces for the four load column signals was very similar in amplitude and time response. The transmitted impulses were calculated by time integration of the pressure-time waveforms. The "dry" side pressure versus time response and the transmitted impulse per unit area waveforms for the different standoff distances have been reported elsewhere [Dharmasena et al. 2007a; Wadley et al. 2007a]. The peak pressure and transmitted impulses for the three standoffs are summarized in Table 1.

4. Finite element simulations

4.1. ***Finite element model of the experimental setup.*** A computational model of the experimental setup was developed to mimic the experiments performed on the dynamically loaded square honeycomb panels, and to study various aspects of the mechanical response of the sandwich panel core. A schematic illustration of the model is shown in Figure 7. In the model, the water, face sheets, specimen tray, and four gage columns were fully meshed using eight-node linear brick elements with reduced integration. Each

Standoff distance (cm)	Peak pressure (MPa)	Transmitted impulse (kPa·s)
25.4	27	6
15.2	40	9.9
10.2	52	11.8

Table 1. Effect of standoff on the transmitted pressure and impulse for solid cylinders.

face sheet was discretized with two elements through the thickness. The honeycomb core walls were meshed using four-node shell elements with finite membrane strains. Five section integration points with Simpson's integration rule were used in each shell element. Fifty elements were uniformly distributed through the core thickness. The core webs were perfectly welded to the face sheet at the corresponding connections. The contact between the bottom surface of the sandwich panel and the top surface of the specimen tray was taken to be frictionless. As suggested by [Wei et al. 2007a; 2007b], the support base beneath the gage columns was modeled as a parallel spring and dashpot pair capable of capturing its elasticity and energy dissipation in terms of its overall response. The top surface of each gage column was perfectly bonded to the specimen tray, while the bottom surface of each gage column was tied to a rigid surface connected to the spring-dashpot pair. The bottom ends of the spring and dashpot were fixed. The base, the spring, and the dashpot were allowed to move only vertically, with no transverse displacements and rotations allowed.

4.2. ***Material properties.*** The water was modeled as an acoustic medium, with a bulk modulus set to 2.05 GPa and a density of 998.23 kg/m^3 [Abaqus 2005]. To model fluid cavitation during reflection of a waterborne impulse with the structure a cavitation pressure was simply set as zero, such that the fluid undergoes free volume expansion when the pressure reaches zero. The sandwich panel was made of a stainless steel alloy having a density of 7900 kg/m^3 and a Poisson ratio of 0.3. In the simulations, the Mises criterion was adopted to model yielding of the material. The true stress (σ) versus true strain (ε)

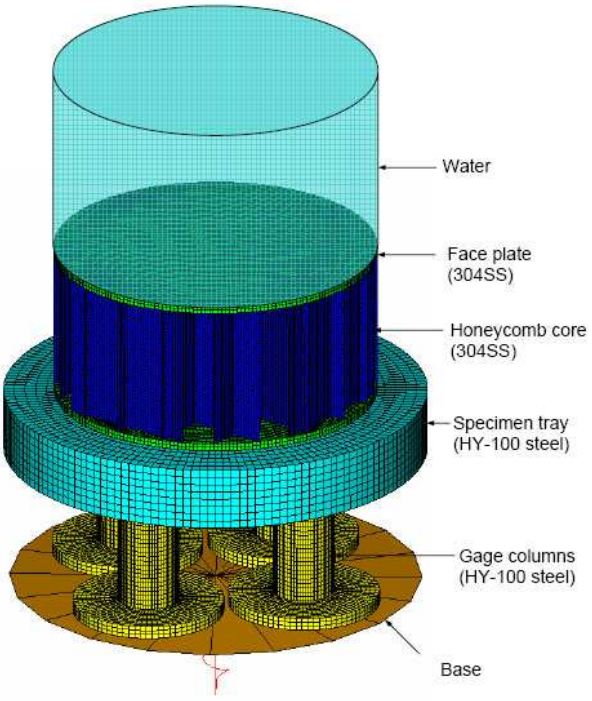

Figure 7. Finite element model representation of the "dynocrusher" test.

relation for the steel was taken to be bilinear for each value of plastic strain-rate, $\dot{\varepsilon}_p$, as

$$\sigma = \begin{cases} E\varepsilon, & \varepsilon \le \dfrac{\sigma_Y}{E}\left(1+\left(\dfrac{\dot{\varepsilon}_p}{\dot{\varepsilon}_0}\right)^m\right), \\ \sigma_Y\left(1+\left(\dfrac{\dot{\varepsilon}_p}{\dot{\varepsilon}_0}\right)^m\right) + E_t\left(\varepsilon - \dfrac{\sigma_Y}{E}\left(1+\left(\dfrac{\dot{\varepsilon}_p}{\dot{\varepsilon}_0}\right)^m\right)\right), & \varepsilon > \dfrac{\sigma_Y}{E}\left(1+\left(\dfrac{\dot{\varepsilon}_p}{\dot{\varepsilon}_0}\right)^m\right). \end{cases}$$

Here, $E = 203\,\text{GPa}$, $\sigma_Y = 176\,\text{MPa}$, and $E_t = 2100\,\text{MPa}$. Dynamic measurements on stainless steels are well represented using the values $\dot{\varepsilon}_0 = 4.916\,\text{s}^{-1}$ and $m = 0.154$. The specimen tray and the gage columns were made of HY100 steel. Since the specimen tray and all the gage columns undergo elastic deformation only, their mechanical behavior was specified by linear elasticity with elastic modulus of 205 GPa, a Poisson ratio of 0.3, and a density of $8000\,\text{kg/m}^3$. All the materials were assumed to be sufficiently ductile that no fracture needed to be taken into account.

In order to calibrate the coefficients of the spring and dashpot, additional finite element simulations were performed for the reference tests, where solid 6061-T6 aluminum alloy cylinders were used as the specimens, as described in Section 4.2. The solid cylinders were fully meshed using eight-node linear brick elements with reduced integration. A density of $2713\,\text{kg/m}^3$ and a Poisson ratio of 0.33 were used for the aluminum alloy cylinder simulations. In addition, its rate dependent stress strain relation was specified by

$$\sigma = \begin{cases} E^{Al}\varepsilon, & \varepsilon \le \dfrac{\sigma_Y^{Al}}{E^{Al}}, \\ \left(\dfrac{E^{Al}-E_t^{Al}}{E^{Al}}\sigma_Y^{Al} + E_t^{Al}\varepsilon\right)\left(1+\left(\dfrac{\dot{\varepsilon}_p^{Al}}{\dot{\varepsilon}_0^{Al}}\right)^m\right), & \varepsilon > \dfrac{\sigma_Y^{Al}}{E^{Al}}, \end{cases}$$

where the elastic modulus $E^{Al} = 70\,\text{GPa}$, the initial yield strength $\sigma_Y^{Al} = 241\,\text{MPa}$, the tangent modulus $E_t^{Al} = 188\,\text{MPa}$, $\dot{\varepsilon}_0 = 163000\,\text{s}^{-1}$, and $m = 1.75$. Other components of the test system were modeled in the same way as discussed before. The calibration procedure for identifying the system compliance is similar to that detailed in [Wei et al. 2007b]. As described in Section 4.2, three calibration tests were performed with the solid cylinders. For a given spring stiffness and dashpot viscosity, the finite element prediction of the transmitted pressure history was compared with the corresponding experimental data. By adjusting the spring stiffness and the dashpot viscosity, the amplitudes of the transmitted signal and echoes and the time intervals of the echoes were reasonably matched. A spring stiffness of 10 GN/m and dashpot viscosity of 1 MN·s/m were found to approximately represent the system compliance.

4.3. ***Hydrocode analysis of the pressure history in water.*** The pressure fields in the fluid and at the specimen-water interface following detonation of an explosive sheet were calculated using a fully coupled Euler–Lagrange finite element hydrocode [Wardlaw and Luton 2000; Wardlaw et al. 2003]. The code allowed the analysis of shock propagation through a fluid medium using an Eulerian solver and then coupled it to the structural response of the solid target using a Lagrange code. Since the explosive sheet was relatively thin (1 mm), and high spatial and temporal gradients of pressure existed in the fluid medium, a fine Eulerian mesh in the direction of the target was used. The Euler run was started with 0.2 mm cells in the explosive sheet thickness direction and 0.4 mm divisions in the other two directions (in the plane parallel to the explosive sheet). The explosive sheet was specified by its geometry, the

explosive's material properties, and by the detonation velocity using the Jones–Wilkins–Lee equations of state for shock calculations [Wardlaw and Luton 2000; Wardlaw et al. 2003]. The pressure loading on a rigid wall, representing the front surface of the solid cylinder, was calculated at four locations along the radial direction measured from the shortest distance of impact of the blast wave.

The time sequences of pressures at various radial distances for standoff distances 25 cm, 15 cm, and 10 cm are shown in Figure 8. They show the pressure at the rigid sample surface as the wave front underwent reflection. These pressure-time histories were then used to apply the necessary loading conditions at the top surface of the water column for the FEM sandwich panel calculations described in Section 4.2.

4.4. ***Numerical investigation on the fundamental dynamics of the unit cell response.*** Due to the periodicity of the square honeycomb core configuration, a simplified finite element model using only one unit cell of the structure can be analyzed, and captures many aspects of dynamic responses of the core [Rabczuk et al. 2004; Xue et al. 2005; Vaziri et al. 2006]. Full three-dimensional models of the square honeycomb unit cell subjected to high intensity loading transmitted through water were developed by detailed meshing of the core. The geometry of the unit cell model was consistent with the samples used in the experimental investigations, and is shown in Figure 9. In this set of calculations, the high intensity loading was simulated as an exponential decay pressure history applied to the top face of the water column, which was modeled using acoustic elements. The material constants required for representing the water characteristics and the sample alloy properties were same as those in Section 4.2. The unit cell model was attached to a fixed rigid plate at its bottom face. In the computational model, the faces and the core webs, as well as the water column, were fully meshed. The boundary conditions applied to the unit cell on the edges of the face sheets and the core webs were consistent with sample symmetry and periodicity. The developed unit cell model is essentially one periodic unit of a plate that is infinite in both directions and which is subject to deformation due a pressure history that is transmitted through water. A second series of simulations were conducted using cells of varying width to assess the effect of the core density, and therefore strength, upon the transmitted pressure. The details of the calculations were similar to previous studies [Rabczuk et al. 2004; Xue et al. 2005; Vaziri et al. 2006].

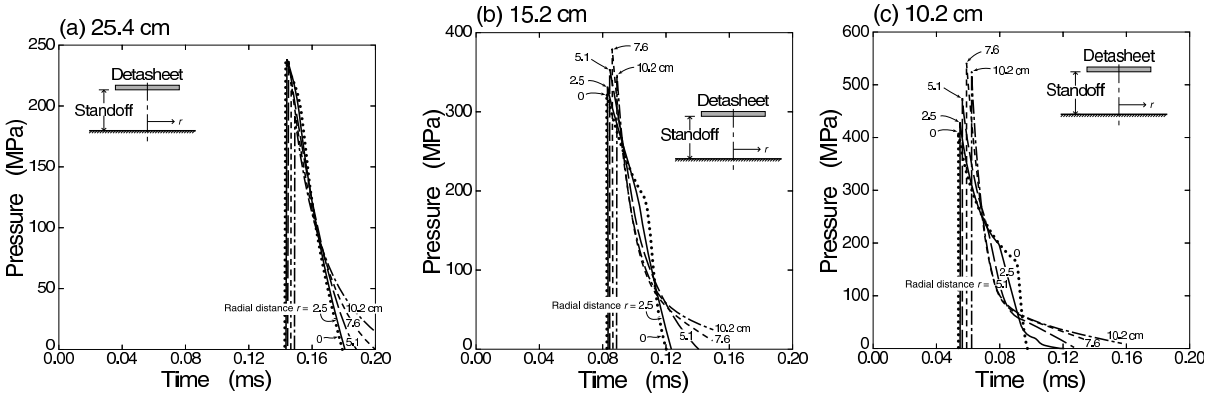

Figure 8. Pressure time loading on a rigid surface calculated from a DYSMAS hydrocode analysis for standoff distances of (a) 25.4 cm, (b) 15.2 cm, and (c) 10.2 cm.

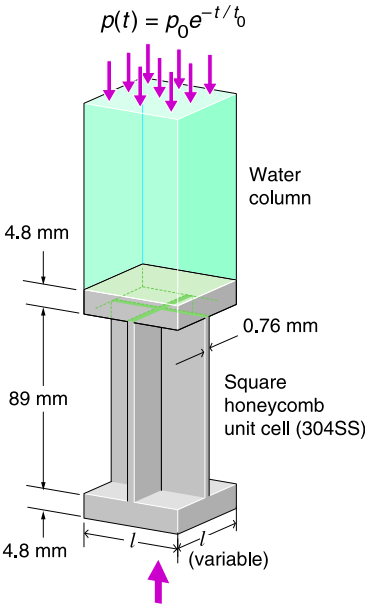

Figure 9. Square honeycomb unit cell finite element model.

5. Results

5.1. ***Sandwich panel responses.*** Figures 10 and 11 show the (dry side) pressure and impulse waveforms for sandwich panel structures following detonations at standoffs of 25.4, 15.2, and 10.2 cm. Both experimental measurements and simulation results (using the approach described in Sections 4.2 and 4.3) from the full 3-dimensional geometry model are shown. The peak pressure measured on the back side of the specimens initially increased and then remained roughly constant as the standoff distance was decreased. At the furthermost standoff of 25.4 cm, the transmitted pressure waveform, Figure 10a, was very similar to that measured on the calibration solid cylinder [Dharmasena et al. 2007a; Wadley et al. 2007a], and consisted of a single dominant peak with weak ringing. The peak pressure was ~ 25 MPa and the maximum transmitted impulse was 5.6 kPa·s. The experimental and full geometry finite element simulation results were generally in good agreement. This sandwich sample exhibited no evidence of permanent buckling or axial compression (verified with measurements of the sample after testing) and was therefore retested at a standoff of 10.2 cm (see Table 2).

Standoff distance (cm)	Peak pressure (MPa)	Transmitted impulse (kPa·s)	Compression (%)
25.4	25	5.6	–
15.2	35	8.2	6.2
10.2	26	9	29

Table 2. Effect of standoff on the experimentally measured transmitted pressure and impulse for a stainless steel, square honeycomb structure with a core relative density of 5%.

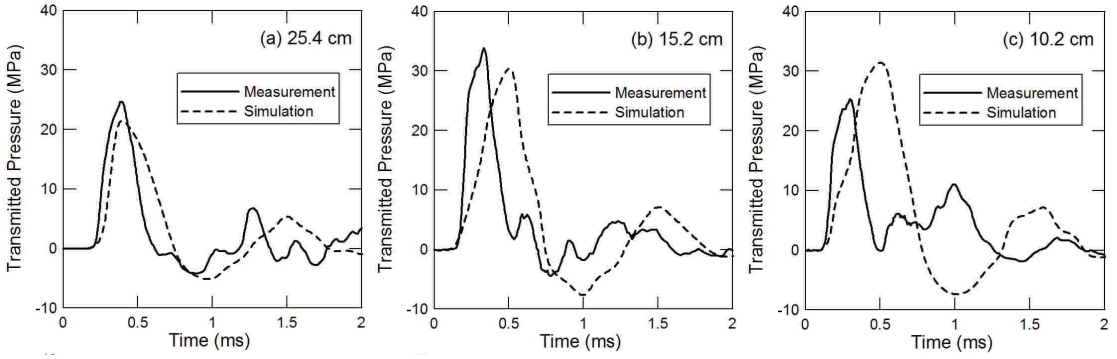

Figure 10. Measured and calculated transmitted pressure-time responses of 304SS square honeycomb core sandwich panels at standoff distances of (a) 25.4 cm, (b) 15.2 cm, and (c) 10.2 cm.

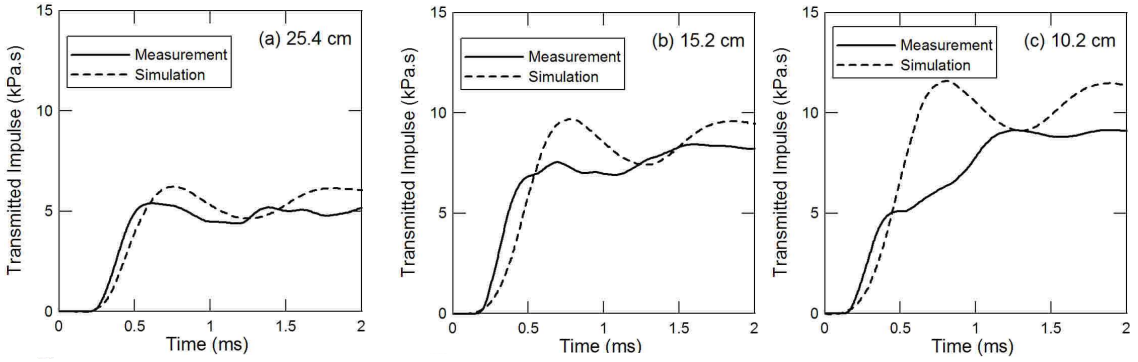

Figure 11. Measured and calculated transmitted impulse time responses of 304SS square honeycomb core sandwich panels at standoff distances of (a) 25.4 cm, (b) 15.2 cm, and (c) 10.2 cm.

Figures 10b and 11b show the dry side pressure and impulse waveforms at a standoff of 15.2 cm. The pressure response consisted of a main pressure peak with a small secondary peak followed by ring down. In this case, the measured peak pressure increased to 35 MPa and the transmitted impulse rose to $\sim$ 8.2 kPa·s (after $\sim$ 2 ms). The secondary peak amplitude was $\sim$ 5 MPa and was delayed by about 0.3 ms from the main pressure peak. The simulated peak pressure and impulse were in good agreement with the experiments. The simulated peak pressure and impulse were $\sim$ 31 MPa and $\sim$ 8.5 kPa·s, respectively. The initial rate of impulse transfer in the simulated response was slightly less than experimentally observed.

A cross sectional view of the sample is shown in Figure 12. The sample suffered an experimentally measured, nonrecoverable axial compressive strain of 6.2%. Cooperative buckling across the full width of the sample occurred close to the bottom (stationary) face. The beginning of a second set of buckles was also evident near the top (wet side) of the specimen.

The pressure and impulse waveforms for a standoff distance of 10.2 cm are shown in Figures 10c and 11c. In this case, three pressure peaks are evident, each separated by about 0.3 ms. The main (first

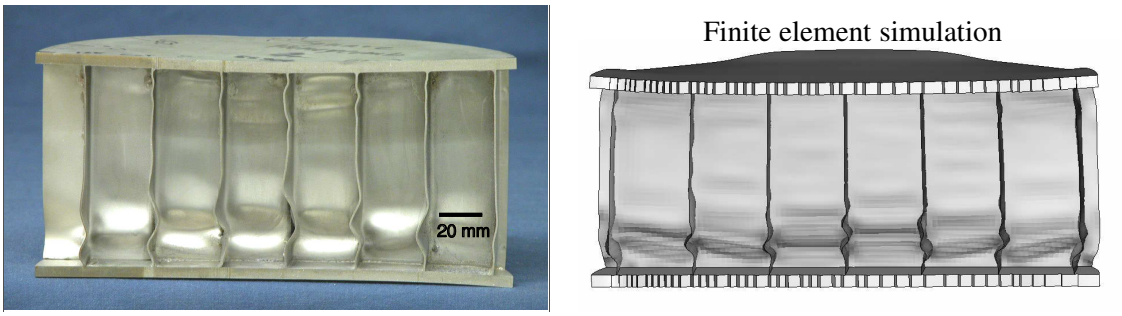

Figure 12. Experimental (left) and predicted (right) cross sections of the final deformed shapes at standoff distance of 15.2 cm.

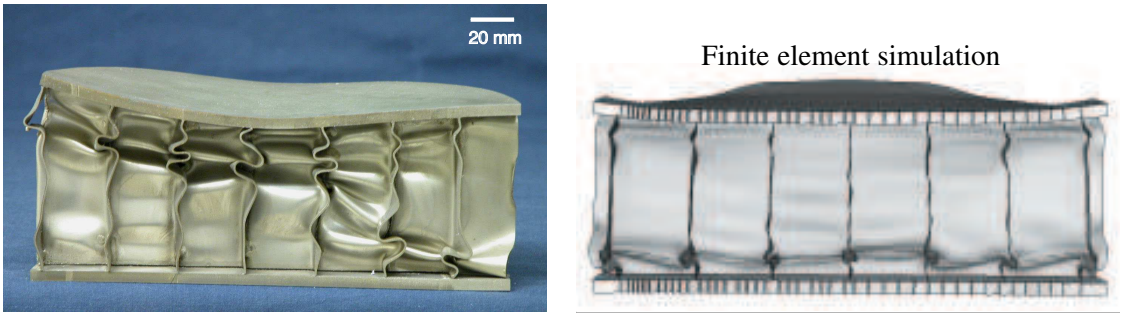

Figure 13. Experimental (left) and predicted (right) cross sections of the final deformed shapes at standoff distance of 10.2 cm.

arriving) peak had a peak pressure of ~ 26 MPa. This was slightly lower than that observed for the 15.2 cm standoff. This first peak was associated with the transfer of about a half the total impulse acquired by the sample. When the two delayed pressure pulses were included, the transmitted impulse after 3 ms reached ~ 9 kPa·s, (see Figure 11c). The predicted pressure response had a first peak of ~ 32 MPa, but failed to capture the two smaller pressure peaks in pressure-time history observed in the experiment (see Figure 10c). The total impulse was, however, similar to that measured experimentally (see Figure 11c). The experiments indicate that core crushing and impulse transfer occurred in two distinct phases, whereas only a single deformation phase was apparent in the simulations.

Cross sectional images of the experimental samples and simulation results help resolve the mechanisms of core response, and the source of the discrepancies between simulations and experiments in the most heavily loaded scenario. Figure 13 shows the cross section of the specimen after testing at the shortest standoff distance. The specimen underwent an axial plastic compressive strain of 29% (measured at the center line). Extensive web buckling is evident with between 2 and 4 folds per web. The intense loading of this sample tripped buckling near both the dry and wet side face sheets. It also resulted in the wet side face sheet debonding from the core consistent with a tensile phase of loading (see Figure 10c between 1.2 and 1.7 ms). Examination of the core interior with the dry side face sheet removed indicated that the peak to peak deflection (amplitude) of the buckles was about 40% of the honeycomb wall spacing.

A cross sectional view of the simulated final deformed configurations of the sandwich panels is also shown in Figures 12 and 13 for standoff distances of 15.2 cm and 10.2 cm. The numerical simulations capture the buckling of the core webs, as well as the face sheet deformation, reasonably well for the 15.2 cm standoff distance. For this case, both the finite element simulation and the experimental results show that the core webs buckle near the bottom face sheet as plastic wave reflection occurs at the bottom face sheet interface. For the 10.2 cm standoff case, the simulation again predicts extensive honeycomb buckling near the bottom face sheet. A much smaller region of buckling near the top face sheet is also evident. However, for the closest standoff (10.2 cm) case, the experiment exhibited buckling at the bottom and top face sheets of roughly similar lateral core web displacement amplitude. At this close standoff, the test sample also exhibited a "dishing" of the front face sheet resulting in more predominant buckles forming at the center of the front face. This observation suggests that with the use of the centrally detonated 20.3 cm $\times$ 20.3 cm explosive sheet (placed above the 20.3 cm diameter test samples), there is a noticeable standoff distance effect on the planarity of the blast wave impacting the test samples. At this highest intensity loading level, it is possible that the second set of buckles near the top face sheet of the tested sample (see Figure 13) contributed to a second distinct phase of impulse transfer in the experimental response, not observed in the simulation result (see Figure 11c). These differences in buckling patterns may be a consequence of imperfections present in the experimental samples but improperly captured in the simulation geometry. The finite element simulations do show a region of significant tensile loading similar to that observed in the experiments. This was presumed to be responsible for top face sheet debonding. Figure 14 shows a time sequence of deformed sandwich panel cross sections for the 10.2 cm standoff, and illustrates the tripping of buckles with progressive folding during the first 0.4 ms of crushing.

The predicted axial crushing strain of the core, defined as the relative displacement between the center of the top and bottom face sheets divided by the original height of core, is plotted in Figure 15a as a function of time. The simulations indicate that it takes around 0.4 ms for the honeycomb core to attain its maximum strain. This corresponds to the period of impulse transfer seen in the experiments (see Figure 11). The values of final crushing strains increased as the standoff distance was decreased, and were reasonably similar to those measured (see Table 3). Figure 15b shows the core crush strain rate as a function of time and the front face velocity (obtained by multiplying the strain rate by the core's original height). It can be seen that the predicted peak front face velocity increased with impulse from $\sim$ 35 m/s to 104 m/s. There is some uncertainty in this estimate for the most intensely loaded experimental test, since the impulse was transferred in two stages while the velocity was deduced from a simulation that assumed more rapid impulse transfer.

Standoff distance (cm)	Experimental core strain (%)	Predicted Core strain (%)
25.4	–	7
15.2	6.2	18
10.2	29	30

Table 3. Comparison of the measured and predicted core strain.

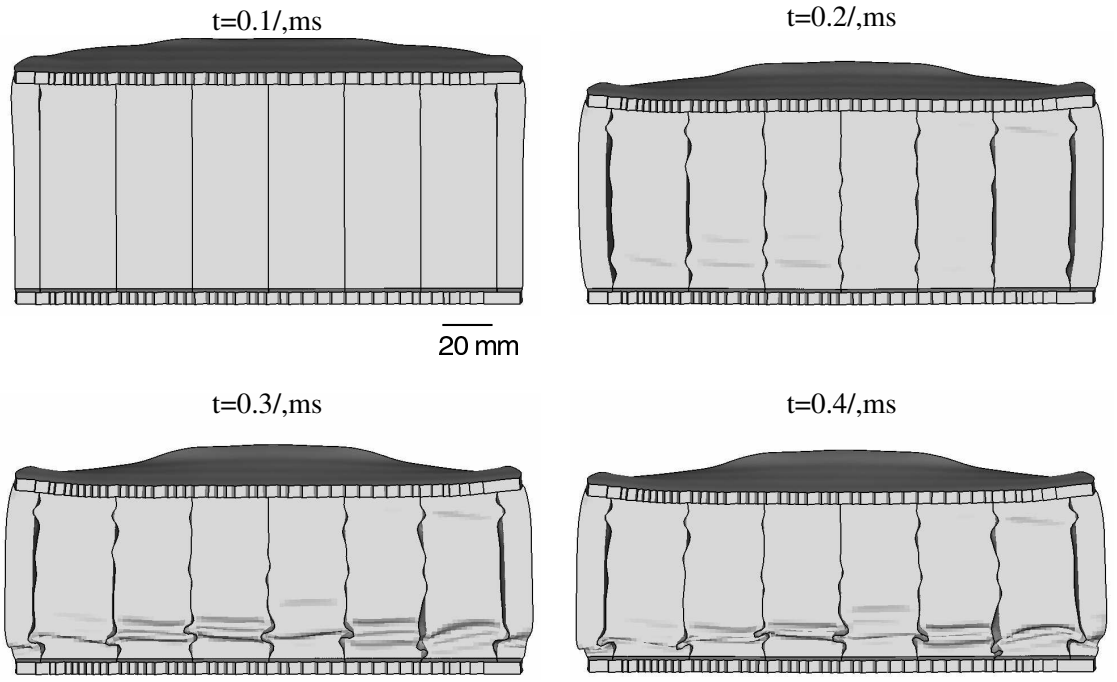

Figure 14. Time sequence of deformed shapes for a sandwich panel tested at the 10.2 cm standoff.

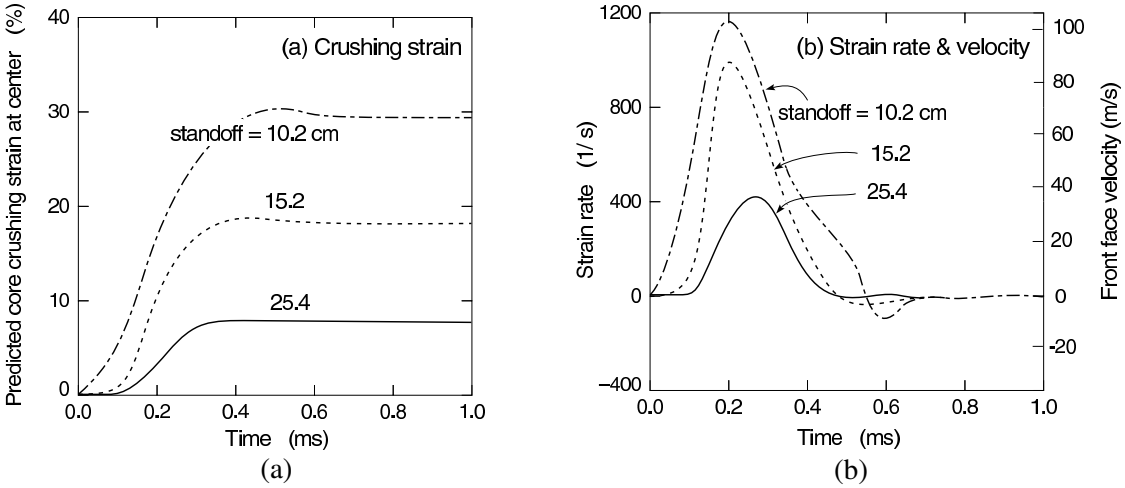

Figure 15. (a) Time dependence of the calculated effective core crushing strain of the square honeycomb panels at standoff distances of 25.4, 15.2, and 10.2 cm. (b) Calculated strain rates and front face velocities for the three standoff distances.

5.2. ***Unit cell simulation results.*** The unit cell computational models were used to investigate the effect of core relative density upon the pressure transmitted by a rigidly supported structure. The face sheet thickness (at 4.8 mm) was held constant to enable the role of the core's crush resistance to be

independently assessed. The core relative density was adjusted by varying the unit cell size (varying the honeycomb cell wall spacing). For each core configuration, the peak load (p_0) was increased from 5 to 200 MPa. In all cases, a characteristic time decay (t_0) of 0.035 ms was chosen to be consistent with that predicted by the hydrocode simulations.

Figure 16 shows the simulation responses for peak overpressures $p_0 = 50$, 100, 150, and 200 MPa, for relative densities between 2 and 7%. For the 7% relative density core (the strongest core analyzed), the peak transmitted pressure increased monotonically from $\sim$ 30 MPa to $\sim$ 52 MPa as the impulse loading was increased from 50 MPa to 200 MPa. For the 5% core, the peak pressure varied from $\sim$21 MPa to $\sim$ 38 MPa over the same overpressure range. Similar monotonic trends were observed from the simulations of the lower core density unit cell samples. These results indicate that very significant reductions in pressure can be achieved when low relative density core structures are used. For example, a 2% relative density core transmits only 16 MPa when impacted by a 200 MPa peak pressure pulse. It can be also seen that the width of the transmitted pressure pulse was inversely related to core density, indicating that the reduction in impulse was not as great as the mitigation of pressure.

Figure 17 summarizes the peak transmitted pressure variation with p_0 for each of the core relative densities. The 7% density strongest core shows a linear relationship with p_0 in the 25–200 MPa range. The 5% core shows an increasing trend with p_0 but at a lower rate of increase than the 7% core. As the core density was further decreased, a weaker dependence of the peak transmitted pressure on p_0 was observed.

6. Discussion

When back supported sandwich panel structures with square honeycomb cores are impulsively loaded in water to a level that is insufficient to cause inelastic core crushing, the transferred impulse and peak pressure are identical to those transmitted through a (back supported) solid plate. It is close to the Taylor predicted limit of $2I_0$ [Taylor 1963]. This has been corroborated by hydrocode simulations of a planar explosive sheet detonated in water at variables distances from a rigid wall [Kiddy 2006]. The experiments reported here indicated that when the incident impulse is able to cause buckling of the honeycomb webs, the transmitted impulse drops significantly from this upper limit even though the back face of the sandwich panel is fully supported and unable to move away from the water borne shock wave.

The effect of the incident overpressure, p_0, and resulting incident impulse strength, I_0, (varied here by changing the standoff) upon the transmitted pressure and impulse are summarized in Figure 18 for the experiments and simulations corresponding to the 3 standoff distances. As the incident impulse was increased to 5 kPa·s (see Figure 18b), core crushing and web buckling were initiated and the transmitted impulse was reduced by 20% compared to that of a solid sample at the same incident impulse. This reduction increased to 25% when the square honeycomb panel was more heavily loaded. In this case, a nearly 30% axial strain occurred in the sample and was accommodated by multiple cell wall buckling events (see Figure 13). This reduction in impulse transfer to the honeycomb sandwich panels arises from the motion of the wet side face sheet away from the incident impulse.

The impulse reductions achieved with honeycomb cores were only a little less than those obtained using pyramidal lattice cores, even though the honeycomb was approximately three times more resistant to quasistatic compression. This higher core strength resulted in a peak pressure transferred by the

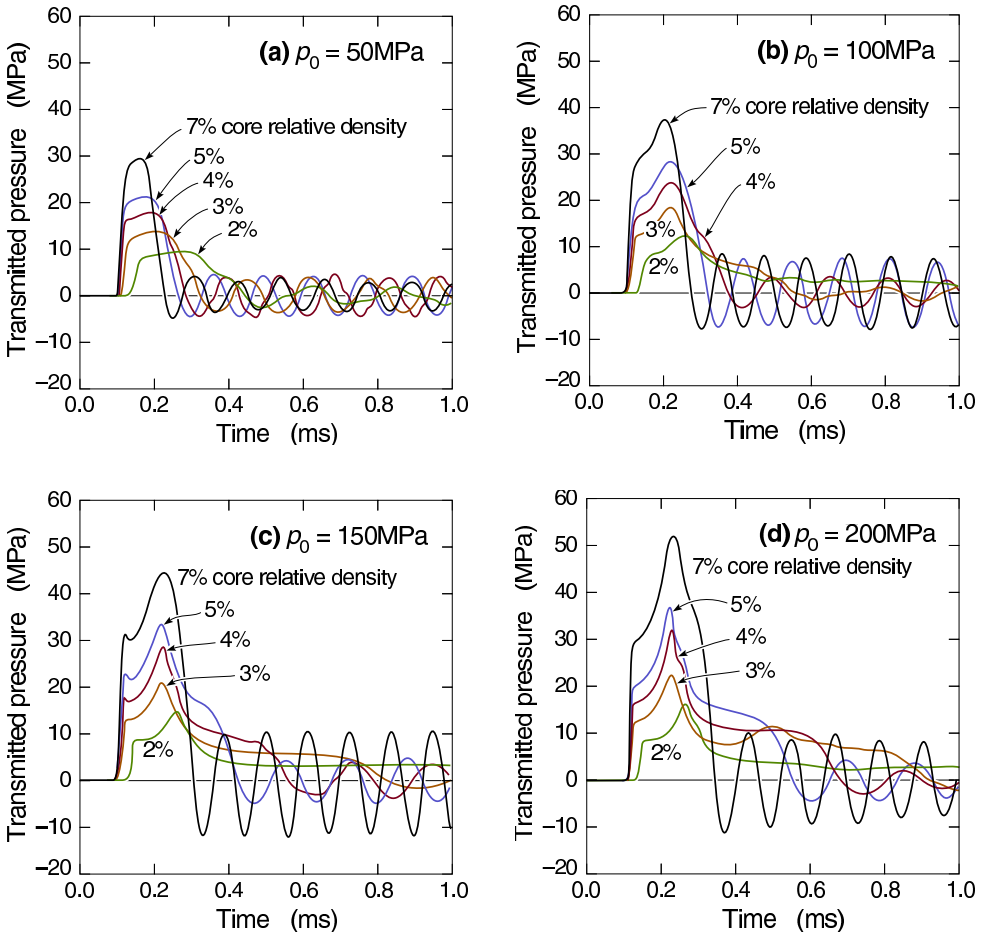

Figure 16. Calculated transmitted pressure response from the unit cell analysis, for different core densities and peak overpressures of (a) 50 MPa, (b) 100 MPa, (c) 150 MPa, and (d) 200 MPa.

honeycomb core (at the 10.2 cm standoff) of $\sim$ 26 MPa, whereas an identically loaded pyramidal lattice structure transmitted only 12 MPa. In the softer core system, the impulse rise time was larger, enabling the total transferred impulse to reach a similar level to that of the honeycomb. Finite element analyses of the honeycomb and pyramidal cores indicate that the maximum transmitted pressure was controlled by the core dynamic strength, which depends upon the core topology and front face velocity during core compression [Deshpande 2006; Radford et al. 2007]. Here, three different impulse loadings (corresponding to three standoff distances) were used and the front face acquired an initial velocity that depended upon the impulse. Figure 15b shows the time derivative of the calculated strain versus time response (see Figure 15a) and the calculated front face velocity of the back supported honeycomb sample of initial core thickness 0.089 m. These velocities were then used with Equation (2) to estimate the dynamic strength elevation of the square honeycomb core. In Table 4 this is compared with the peak pressure deduced strengths (scaled by that measured quasistatically) for the three standoff distances. Reasonable

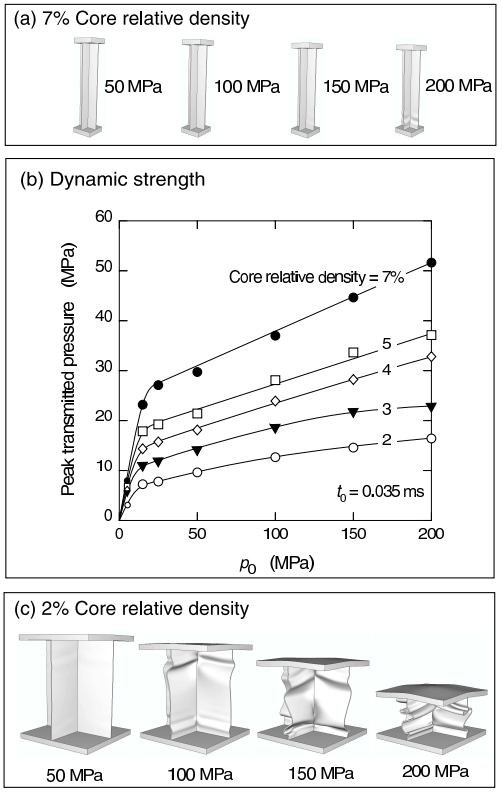

Figure 17. Deformed configurations for the 7% (a) and 2% (c) density square honeycomb unit cells. The peak transmitted back face pressure variation with overpressures (p_0), for a core density range of 2–7% (b).

agreement is observed for the two larger standoff cases, whereas the shorter standoff experiment is again consistent with a slower impulse transfer process.

Significant pressure reductions can be achieved by lowering the core relative density as illustrated in Figure 17. However, for a given impulse load, increasing crush displacements are reached as the core relative density (strength) is reduced. If core densification occurs, the impulse carried by the front face is transferred to the supports, which then experience much higher pressure levels. This can be avoided by designing sandwich panels to have a core thickness above an impulse dependent minimum value. In

Standoff distance (cm)	Calculated front face velocity (m/s)	Dynamic/quasistatic strength ratio	
		Predicted	Measured
25.4	35.6	1.73	2.08
15.2	88.9	2.98	2.92
10.2	103.7	3.32	2.12

Table 4. Effect of standoff on the front face velocity and the dynamic to static strength ratio of the square honeycomb core.

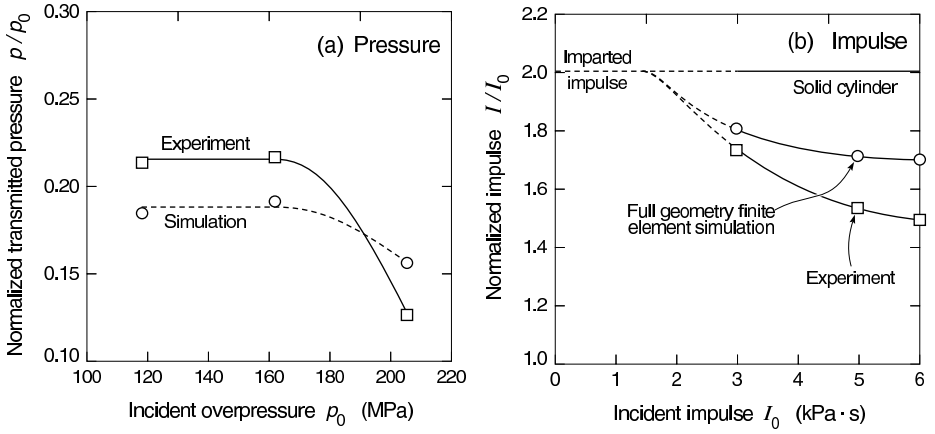

Figure 18. (a) The dependence of the transmitted pressure upon incident pressure. (b) The variation of the transmitted impulse with incident impulse.

this case, the transmitted pressure is controlled by the dynamic crush strength of the core, σ_{cD}. The required minimum thickness for the cellular core, $h_{\min}$, can be estimated from [Ashby et al. 2000] and [Wadley et al. 2007b] as

$$h_{\min} = \frac{I^2}{2m_f \sigma_{cD}(1-\bar{\rho})},$$

where I is the impulse (momentum) per unit area imparted to the sandwich panel, m_f the mass per unit area of the front face sheet, $\bar{\rho}$ the core relative density, and σ_{cD} the dynamic crush strength of the core before densification is reached.

7. Summary

A combined experimental and computational simulation approach has been used to investigate impulse transfer during underwater shock loading of back supported sandwich structures with square honeycomb core topologies. The study indicates that significant impulse reductions occur, provided core crushing is activated. The majority of the core crushing in square honeycomb core panels occurs by web buckling. This appears to initiate at the dry side face sheet-web interface upon plastic wave reflection. The impulse transferred to these sandwich panels lies below the Taylor predicted limit ($2p_0t_0$) for a rigidly supported plate and above that of a free plate with mass per unit area corresponding to the wet side face sheet. The impulse transferred to the square honeycomb panels was slightly higher than that transferred to pyramidal core structures whose crush strength is lower than the honeycomb. The experimental study indicates that the transmitted impulse rise time was increased in the sandwich panel systems. This appears to result from the sequential tripping of regions of buckling within the most intensely loaded test structures. For a fixed impulse, increasing the rise time of the transmitted impulse reduces the transmitted pressure and provides beneficial dynamic pulse mitigation effects. “Weaker” core designs (for example a multilayer lattice structure) enhance this beneficial feature, and reduce both the transmitted peak pressure and the impulse under similar loading conditions. The fluid structure interaction for a sandwich panel is influenced by the properties of the fluid medium, the thickness and the density of the face sheet, and

the topology and strength of the sandwich core. Using a unit cell analysis, the face sheet has been kept constant, and the core strength adjusted systematically by varying the core relative density. This has enabled the investigation of the effects of the core strength on the transmitted pressure to a back supported structure. It shows that the core relative density (for a selected sandwich core topology) can be effectively used as a parameter to control the transmitted pressure, provided an adequate core thickness can be used.

Acknowledgements

This research was supported by the Office of Naval Research grant number N00014-03-1-0281 monitored by Drs. Edward Johnson and Daniel Tam, and the Blast Resistant Materials program monitored by Drs. Steve Fishman and David Shifler (grant number N00014-01-1-1051). Zhenyu Xue and Ashkan Vaziri were also supported in part by the Office of Naval Research under grants N00014-02-1-0700 and GG10376-114934 and in part by the School of Engineering and Applied Sciences, Harvard University. We are grateful to Profs. John W. Hutchinson and Vikram Deshpande for many insightful discussions.

References

[Abaqus 2005] Hibbit, Karlsson and Sorensen Inc., *ABAQUS/Explicit User's Manual*, Hibbit, Karlsson and Sorensen Inc., 2005. Version 6.0.

[Ashby et al. 2000] M. F. Ashby, A. G. Evans, N. A. Fleck, L. J. Gibson, J. W. Hutchinson, and H. N. G. Wadley, *Metal foams: a design guide*, Butterworth-Heinemann, 2000.

[Baker et al. 1998] W. E. Baker, T. C. Togami, and J. C. Weyder, "Static and dynamic properties of high-density metal honeycombs", *Int. J. Impact Eng.* **21**:3 (1998), 149–163.

[Cole 1948] R. H. Cole, *Underwater explosions*, Princeton University Press, 1948.

[Deshpande 2006] V. S. Deshpande, Private communication, 2006.

[Deshpande and Fleck 2005] V. S. Deshpande and N. A. Fleck, "One-dimensional shock response of sandwich plates", *J. Mech. Phys. Solids* **53** (2005), 2347–2383.

[Deshpande et al. 2006] V. S. Deshpande, A. Heaver, and N. A. Fleck, "An underwater shock simulator", *Proc. Royal Soc. A* **462** (2006), 1021–1041.

[Dharmasena et al. 2007a] K. P. Dharmasena, D. T. Queheillalt, H. N. G. Wadley, Y. Chen, P. Dudt, D. Knight, Z. Wei, and A. G. Evans, "Dynamic response of a multilayer prismatic structure to impulsive loads incident from water", *Int. J. Impact Eng.* (2007). accepted.

[Dharmasena et al. 2007b] K. P. Dharmasena, H. N. G. Wadley, Z. Xue, and J. W. Hutchinson, "Mechanical response of metallic honeycomb sandwich panel structures to high-intensity dynamic loading", *Int. J. Impact Eng.* (2007).

[Fleck and Deshpande 2004] N. A. Fleck and V. S. Deshpande, "The resistance of clamped sandwich beams to shock loading", *J. Appl. Mech.* **71** (2004), 386–401.

[Hutchinson and Xue 2005] J. W. Hutchinson and Z. Xue, "Metal sandwich plates optimized for pressure impulses", *Int. J. Mech. Sci.* **47** (2005), 545–569.

[Kambouchev et al. 2006] N. Kambouchev, L. Noels, and R. Radovitzky, "Compressibility effects on fluid-structure interactions and their implications on the blast loading of structures", *J. Appl. Phys.* **100**:6 (2006), 063519.

[Kiddy 2006] K. Kiddy, Private communication, 2006.

[Lee et al. 2006a] S. Lee, F. Barthelat, J. W. Hutchinson, and H. D. Espinosa, "Dynamic failure of pyramidal truss core materials—experiments and modeling", *Int. J. Plast.* **22** (2006), 2118–2145.

[Lee et al. 2006b] S. Lee, F. Barthelat, N. Moldovan, H. D. Espinosa, and H. N. G. Wadley, "Deformation rate effects on failure modes of open-cell Al foams and textile cellular materials", *Int. J. Solids Struct.* **43** (2006), 53–73.

[Liang et al. 2007] Y. Liang, A. V. Spuskanyuk, S. E. Flores, D. R. Hayhurst, J. W. Hutchinson, R. M. McMeeking, and A. G. Evans, "The response of metallic sandwich panels to water blast", *J. Appl. Mech. (Trans. ASME)* **74**:1 (2007), 81–99.

[McShane et al. 2007] G. McShane, V. S. Deshpande, and N. A. Fleck, "The underwater blast resistance of metallic sandwich beams with prismatic lattice cores", *J. Appl. Mech. (Trans. ASME)* **74** (2007), 352–364.

[Mori et al. 2007] L. Mori, S. Lee, Z. Xue, A. Vaziri, D. T. Queheillalt, K. P. Dharmasena, H. N. G. Wadley, J. W. Hutchinson, and H. D. Espinosa, "Deformation and fracture modes of sandwich structures subjected to underwater impulsive loads", *J. Mech. Mater. Struct.* (2007). In press.

[Qiu et al. 2003] X. Qiu, V. S. Deshpande, and N. A. Fleck, "Finite element analysis of the dynamic response of clamped sandwich beams", *Eur. J. Mech. A/Solids* **22**:6 (2003), 801–814.

[Rabczuk et al. 2004] T. Rabczuk, J. Y. Kim, E. Samaniego, and T. Belytschko, "Homogenization of sandwich structures", *Int. J. Numer. Methods Eng.* **61** (2004), 1009–1027.

[Radford et al. 2005] D. D. Radford, V. S. Deshpande, and N. A. Fleck, "The use of metal foam projectiles to simulate shock loading on a structure", *Int. J. Impact Eng.* **31**:9 (2005), 1152–1171.

[Radford et al. 2007] D. D. Radford, G. J. McShane, V. S. Deshpande, and N. A. Fleck, "Dynamic compressive response of stainless-steel square honeycombs", *J. Appl. Mech.* **74** (2007), 658–667.

[Rathbun et al. 2006] H. J. Rathbun, D. D. Radford, Z. Xue, M. Y. He, J. Yang, V. S. Deshpande, N. A. Fleck, J. W. Hutchinson, F. W. Zok, and A. G. Evans, "Performance of metallic honeycomb-core sandwich beams under shock loading", *Int. J. Solids Struct.* **43** (2006), 1746–1763.

[Stout and Follansbee 1986] M. G. Stout and P. S. Follansbee, "Strain rate sensitivity, strain hardening, and yield behavior of 304L stainless steel", *J. Eng. Mater. Technol. (Trans. ASME)* **108** (1986), 344–353.

[Taylor 1963] G. I. Taylor, "The scientific papers of G. I. Taylor", pp. 287–303 in *The pressure and impulse of submarine explosion waves on plates*, vol. volume III, Cambridge University Press, Cambridge, 1963.

[Tilbrook et al. 2006] M. T. Tilbrook, V. S. Deshpande, and N. A. Fleck, "The impulsive response of sandwich beams: Analytical and numerical investigation of regimes of behaviour", *J. Mech. Phys. Solids* **54** (2006), 2242–2280.

[Vaughn and Hutchinson 2006] D. G. Vaughn and J. W. Hutchinson, "Bucklewaves", *Eur. J. Mech. A: Solids* **25** (2006), 1–12.

[Vaziri and Hutchinson 2007] A. Vaziri and J. W. Hutchinson, "Metallic sandwich plates subject to intense air shocks", *Int. J. Solids Struct.* **44** (2007), 2021–2035.

[Vaziri and Xue 2007] A. Vaziri and Z. Xue, "Mechanical behavior and constitutive modeling of metal cores", *J. Mech. Mater. Struct.* (2007). in press.

[Vaziri et al. 2006] A. Vaziri, Z. Xue, and J. W. Hutchinson, "Metal sandwich plates with polymer foam-filled cores", *J. Mech. Mater. Struct.* **1** (2006), 95–125.

[Wadley 2006] H. N. G. Wadley, "Multifunctional periodic cellular materials", *Phil. Trans. R. Soc. A* **364** (2006), 31–68.

[Wadley et al. 2003] H. N. G. Wadley, A. G. Evans, and N. A. Fleck, "Fabrication and structural performance of periodic cellular metal sandwich structures", *Compos. Sci. Tech.* **63**:16 (2003), 2331–2343.

[Wadley et al. 2007a] H. N. G. Wadley, K. P. Dharmasena, Y. Chen, P. Dudt, D. Knight, R. Charette, and K. Kiddy, "Compressive response of multilayered pyramidal lattices during underwater shock loading", *Int. J. Impact Eng.* (2007).

[Wadley et al. 2007b] H. N. G. Wadley, K. P. Dharmasena, M. He, R. McMeeking, A. G. Evans, N. Kambouchev, and R. Radovitzky, *Cellular materials concepts for air blast mitigation*, 2007. In preparation.

[Wardlaw and Luton 2000] A. J. Wardlaw and J. A. Luton, "Fluid-structure interaction mechanisms for close-in explosions", *Shock Vib. J.* **7** (2000), 265–275.

[Wardlaw et al. 2003] A. J. Wardlaw, J. Luton, J. J. Renzi, and K. Kiddy, "Fluid-structure coupling methodology for undersea weapons", pp. 251–263 in *Fluid Structure Interaction II*, WIT Press, 2003.

[Wei et al. 2007a] Z. Wei, A. G. Evans, K. P. Dharmasena, and H. N. G. Wadley, "Analysis and interpretation of a test for characterizing the response of sandwich panels to water blast", *Int. J. Impact Eng.* **34** (2007), 1602–1618.

[Wei et al. 2007b] Z. Wei, M. Y. He, and A. G. Evans, "Application of a dynamic constitutive law to multilayer metallic sandwich panels subject to impulsive loads", *J. Appl. Mech.* **74** (2007), 636–644.

[Xue and Hutchinson 2004] Z. Xue and J. W. Hutchinson, "A comparative study of impulse-resistant metal sandwich plates", *Int. J. Impact Eng.* **30** (2004), 1283–1305.

[Xue and Hutchinson 2006] Z. Xue and J. W. Hutchinson, "Crush dynamics of square honeycomb sandwich cores", *Int. J. Numer. Methods Eng.* **65** (2006), 2221–2245.

[Xue et al. 2005] Z. Xue, A. Vaziri, and J. W. Hutchinson, "Non-uniform constitutive model for compressible orthotropic materials with application to sandwich plate cores", *Cmes-Comp. Model. Eng.* **10** (2005), 79–95.

Received 6 Sep 2007. Revised 6 Sep 2007.

Please
accept

HAYDN N. G. WADLEY: haydn@virginia.edu
Department of Materials Science and Engineering, University of Virginia, 395 McCormick Road, Charlottesville VA 22904, United States

KUMAR P. DHARMASENA: kumar@virginia.edu
Department of Materials Science and Engineering, University of Virginia, 395 McCormick Road, Charlottesville VA 22904, United States

DOUG T. QUEHEILLALT: dtq2j@virginia.edu
Department of Materials Science and Engineering, University of Virginia, 395 McCormick Road, Charlottesville VA 22904, United States

YUNGCHIA CHEN: yungchia.chen@navy.mil
Naval Surface Warfare Center, Carderock Division, West Bethesda MD 20817, United States

PHILIP DUDT: philip.dudt@navy.mil
Naval Surface Warfare Center, Carderock Division, West Bethesda MD 20817, United States

DAVID KNIGHT: david.e.knight@navy.mil
Naval Surface Warfare Center, Carderock Division, West Bethesda MD 20817, United States

KEN KIDDY: kenneth.kiddy@navy.mil
Naval Surface Warfare Center, Indian Head Division, Indian Head MD 20640, United States

ZHENYU XUE: xue@deas.harvard.edu
School of Engineering and Applied Sciences, Harvard University, Cambridge MA 02138, United States

ASHKAN VAZIRI: avaziri@deas.harvard.edu
School of Engineering and Applied Sciences, Harvard University, Cambridge MA 02138, United States